Am J Physiol Renal Physiol 292: F456–F466, 2007.
First published August 8, 2006; doi:10.1152/ajprenal.00087.2006.

Cellular distribution of the potassium channel KCNQ1 in normal mouse kidney

Wencui Zheng,[2] Jill W. Verlander,[2] I. Jeanette Lynch,[2] Melanie Cash,[1] Jiahong Shao,[2] Lisa R. Stow,[2] Brian D. Cain,[2] I. David Weiner,[1,2] Susan M. Wall,[3] and Charles S. Wingo[1,2]

[1]*North Florida/South Georgia Veterans Health System,* [2]*University of Florida College of Medicine, Gainesville, Florida, and* [3]*Emory University Renal Division, Atlanta, Georgia*

Submitted 15 March 2006; accepted in final form 20 July 2006

Zheng W, Verlander JW, Lynch IJ, Cash M, Shao J, Stow LR, Cain BD, Weiner ID, Wall SM, Wingo CS. Cellular distribution of the potassium channel KCNQ1 in normal mouse kidney. *Am J Physiol Renal Physiol* 292: F456–F466, 2007. First published August 8, 2006; doi:10.1152/ajprenal.00087.2006.—Mechanisms of K^+ secretion and absorption along the collecting duct are not understood fully. Because KCNQ1 participates in K^+ secretion within the inner ear and stomach, distribution of KCNQ1 in mouse kidney was studied using Northern and Western analyses, RT-PCR of isolated tubules, and immunohistochemistry. Northern blots demonstrated KCNQ1 transcripts in whole kidney. RT-PCR showed KCNQ1 mRNA in isolated distal convoluted tubule (DCT), connecting segment (CNT), collecting ducts (CD), and glomeruli. Immunoblots of kidney and stomach revealed a ~75-kDa protein, the expected mobility for KCNQ1. KCNQ1 was detected by immunohistochemistry throughout the distal nephron and CD. Thick ascending limbs exhibited weak basolateral immunolabel. In DCT and CNT cells, immunolabel was intense and basolateral, although KCNQ1 label was stronger in late than in early DCT. Initial collecting tubule and cortical CD KCNQ1 immunolabel was predominantly diffuse, but many cells exhibited discrete apical label. Double-labeling experiments demonstrated that principal cells, type B intercalated cells, and a few type A intercalated cells exhibited distinct apical KCNQ1 immunolabel. In inner medullary CD, principal cells exhibited distinct basolateral KCNQ1 immunolabel, whereas intercalated cells showed diffuse cytoplasmic staining. Thus KCNQ1 protein is widely distributed in mouse distal nephron and CD, with significant axial and cellular heterogeneity in location and intensity. These findings suggest that KCNQ1 has cell-specific roles in renal ion transport and may participate in K^+ secretion and/or absorption along the thick ascending limb, DCT, connecting tubule, and CD.

KvLQT1; Kv7.1; slowly activating potassium channel

KCNQ1, also known as KvLQT1 and Kv7.1, is the pore-forming α-subunit of the $I_{KS}K^+$ channel (17), a delayed rectifier voltage-gated K^+ channel (4, 15, 16) that enables a K^+ current after electrical depolarization of the cell membrane in the heart (8). Mutations of KCNQ1 in humans cause dysfunction of the slowly activating K^+ channel in the heart and produce long QT syndrome (23, 25, 28, 29, 32, 40). In the inner ear, KCNQ1 mediates K^+ secretion into the endolymph, which is important for normal inner ear function (5, 31). Humans with certain KCNQ1 gene mutations exhibit the autosomal recessive Jervell and Lange-Nielsen syndrome, which is manifested as hearing loss in addition to cardiac conduction abnormalities (6, 41). KCNQ1-homozygous mutant mice also exhibit cochlear deafness, as well as circling, head bobbing, and inability to right themselves during a fall, indicative of vestibular dysfunction (5, 19).

KCNQ1 is also expressed in the stomach (9, 20), where it colocalizes with H^+-K^+-ATPase in the parietal cell canaliculus (19) and is necessary for gastric acid secretion. Genomic microarray analysis of isolated gastric cells identified KCNQ1 as a likely candidate for the K^+-efflux channel associated with H^+-K^+-ATPase in the stomach (19). KCNQ1-knockout mice exhibit hypochlorhydria, hypergastrinemia, gastric hyperplasia, and vacuolation of the parietal cells, all of which suggest that KCNQ1 is necessary for normal gastric acid secretion (10, 20). In addition, pharmacological inhibition of KCNQ1 blocks gastric acid secretion in normal rat and dog stomach and in isolated rabbit gastric glands (10, 19). The dependence of H^+-K^+-ATPase function on KCNQ1 in the gastric parietal cell suggests that a similar relation may exist in renal collecting duct cells that express H^+-K^+-ATPase.

The presence of KCNQ1 in the kidney has been demonstrated by RT-PCR (20), immunofluorescence, and in situ hybridization (7). Use of antibodies raised against a peptide from the amino terminus of human KCNQ1 resulted in detection of KCNQ1 immunoreactivity only in the proximal tubule brush border (33). Furthermore, recent physiological studies provide functional evidence that KCNQ1 enhances Na^+-dependent transport in the proximal tubule, presumably by contributing to a favorable electrical gradient for Na^+ uptake (34). These observations appear to conflict with in situ hybridization studies that found KCNQ1 mRNA in distal tubules and collecting ducts in the cortex and medulla but not in proximal tubules (7).

Thus the purpose of this study was to determine the tubule- and cell-specific location of KCNQ1 mRNA and protein in mouse kidney with use of probes against the 3′ end of KCNQ1 mRNA and the carboxy terminus of human KCNQ1 protein.

METHODS

Animals

Adult (19–28 g body wt) C57BL/6 mice ($n = 4$) were used for immunoblot analysis, immunohistochemistry, Northern analysis, and RT-PCR studies. Adult 129 Black Swiss mice ($n = 3$) and C3H/HeJCrl-Kcnq1 mice (Jackson Laboratory, Bar Harbor, ME) expressing the mutant KCNQ1 phenotype of head bobbing, circling, and tumbling ($n = 3$) or the wild-type phenotype ($n = 3$) were also used for immunohistochemistry. All animal use was in compliance with the American Physiological Society "Guiding Principles in the Care and

Address for reprint requests and other correspondence: C. S. Wingo, VAMC, 1601 SW Archer Rd., Research 151, Gainesville, FL 32608 (e-mail: cswingo@ufl.edu).

The costs of publication of this article were defrayed in part by the payment of page charges. The article must therefore be hereby marked "*advertisement*" in accordance with 18 U.S.C. Section 1734 solely to indicate this fact.

Use of Animals," and animal use protocols were approved by the North Florida/South Georgia Veterans Administration Institutional Animal Care and Use Committee.

Tubule Dissection

Inner medullary collecting ducts (IMCD), outer medullary collecting ducts (OMCD), cortical collecting ducts (CCD), connecting segment (CNT), distal convoluted tubules (DCT), cortical thick ascending limb (cTAL), proximal tubules, and glomeruli were dissected in cold DMEM-Ham's F-12 with HEPES buffer (Invitrogen, Carlsbad, CA) containing 0.25 mg/ml collagenase type I (Sigma Aldrich, St. Louis, MO), 5 mM glycine, 50 U/ml DNase I, and 50 μg/ml soybean trypsin inhibitor. Transverse slices of the kidney through the hilum were dissected to separate the cortex, outer medulla, and inner medulla. The slices were incubated at 37°C and gently agitated for 30 min (cortex and outer medulla) and 2 h (inner medulla). The tubules were then sedimented on ice for 5 min. The supernatant was replaced with neutralization solution containing 1% BSA in DMEM-Ham's F-12 with HEPES buffer. The tubule-rich suspensions were gently transferred via pipette to a dissection dish containing DMEM-Ham's F-12 with HEPES buffer and 0.1% BSA. Tubules were sorted with a 30-gauge needle at ~2°C under a stereomicroscope. Three segments of the proximal tubule were dissected: the proximal straight tubule in the cortex and the early and late proximal convoluted tubules. The proximal straight tubule was identified and dissected up to the late proximal convoluted tubule, which was separated from the straight portion. The early proximal convoluted tubule was dissected from its point of connection with Bowman's capsule. The DCT, CNT, and CCD were identified with branch points connecting distal tubules and connecting tubules with CCD. For the DCT, the bright convoluted portions of the distal tubules were used. The CNT was identified as the granular portion of the distal tubules and the CCD as the segment below the last branch point. cTAL were identified by their narrow diameter, rigidity, and bright, reflective appearance. OMCD was distinguished from the medullary thick ascending limb (TAL) on the basis of its granular and nonreflective appearance. IMCD were identified by their relatively large diameter compared with all other structures in the inner medulla. The tubules were placed into individual 1.5-ml microcentrifuge tubes in buffer and stored at −70°C.

RNA Isolation and RT-PCR

Whole kidney total RNA was extracted using TRIzol reagent (Invitrogen, Carlsbad, CA) according to the manufacturer's instructions. The RT reaction was performed according to the manufacturer's instructions, with ~500 ng of RNA, determined by optical density reading at 260 nm, and oligo(dT) and Superscript II RT (Invitrogen). The resulting cDNA was used for the second-strand synthesis with gene-specific primers to 940 bp of the coding region of KCNQ1 [accession no. BC055304; 5′-ctgtacattggctttctgggccttatct-3′ (sense) and 5′-ttttctgagatggggatgaacaaagatg-3′ (antisense)] under the following conditions: an initial hot start at 94°C for 1 min to activate the Advantage cDNA polymerase (BD Biosciences Clontech, Palo Alto, CA) and 30 cycles at 94°C for 30 s, 60°C for 30 s, and 72°C for 3 min, with a final extension at 72°C for 10 min. The second-strand reaction was used as a template in a subsequent reaction under the conditions described above. The resultant PCR products were separated by gel electrophoresis on a 1.2% agarose gel and detected by 0.1% ethidium bromide. The PCR products were cloned and submitted to the University of Florida Interdepartmental Core for Biotechnology Research for DNA sequencing.

Tubule total RNA was extracted as described above using 800 μl of TRIzol (Invitrogen). Oligo(dT) primers and Superscript III RT (Invitrogen) were used to make cDNA from 200 ng of RNA from each nephron segment, except in one experiment, where only 90 ng of RNA were used for the early proximal convoluted tubule because of low tubule yield. The cDNA was then used as a template for PCR amplification using the gene-specific primers for KCNQ1, as for whole kidney, and for GAPDH using 5′-agacacgatggtgaaggtcggagtgaac-3′ (sense) and 5′-gtggcactgttgaagtcgcaggag-3′ (antisense), which yields a 860-bp product. All PCRs were carried out in the presence or absence of RT to check for genomic DNA contamination and were amplified as follows: initial hot start cycle at 94°C for 1 min to activate the Advantage cDNA polymerase (BD Biosciences Clontech) and 35 cycles at 94°C for 30 s, 60°C for 30 s, and 72°C for 3 min, with a final extension cycle at 72°C for 10 min. PCR products were electrophoresed on a 1.5% agarose gel and visualized with 0.1% ethidium bromide.

Northern Analyses

Total kidney RNA (20 μg) was prepared for Northern analysis using glyoxalation (27). After 50 min at 50°C, the RNA was electrophoresed at 200 mA (110 V) for 90 min. The ribosomal bands were visualized using ethidium bromide and the RNA was transferred to a Hybond-N nylon membrane (Amersham, Little Chalfont, Buckinghamshire, UK) in 10× saline-sodium citrate [1.5 M NaCl and 150 mM sodium citrate (pH 7.0)] over ~16 h. The KCNQ1 probe was synthesized using the Prime-It RmT random primer labeling kit (catalog no. 300392, Stratagene, La Jolla, CA) and 200 ng of KCNQ1 insert [bp 793–1733 in the coding sequence (accession no. BC055304)] with 3,000 Ci/mmol [α-^{32}P]dCTP (Perkin Elmer Life Sciences, Shelton, CT). For hybridization, the membrane was incubated with the KCNQ1 probe for ~16 h and then washed three times for 30 min each in 300 ml of wash buffer [20 mM Na_2HPO_4, 10 mM SDS, and 1 mM EDTA (pH 7.2)] at 65°C. The signal was recorded on Kodak Biomax MS scientific imaging film by exposure to the membrane for 6 days.

Membrane Protein Extraction and Immunoblot Analysis

A membrane vesicle preparation (15) was used to extract total protein from whole kidney and whole stomach. Protein concentration was measured using bicinchoninic acid reagents (Pierce, Rockford, IL) according to the manufacturer's instructions. The protein samples were diluted 1:1 with sample dilution buffer containing 5% β-mercaptoethanol (Bio-Rad, Hercules, CA) and denatured for 5 min before separation on a 10% Tris·HCl PAGE ready-gel (Bio-Rad) at 18 mA for 90 min; molecular sizes were estimated using High-Range Rainbow molecular weight markers (catalog no. RPN756, Amersham Biosciences) loaded on the same gel. The gel was electrophoretically transferred to a polyvinylidene difluoride membrane at 250 mA for 60

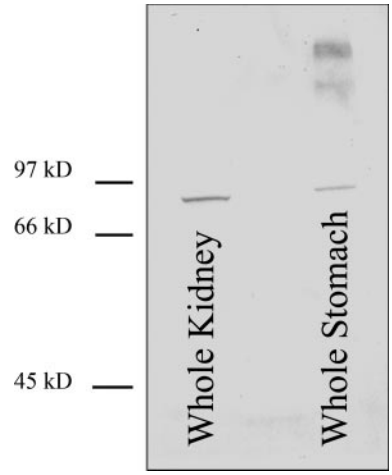

Fig. 1. Immunoblot analysis of membrane protein isolated from kidney and stomach. Immunoreactive protein was detected by the KCNQ1 antibody at ~75 kDa, the expected mobility for KCNQ1. Molecular size markers are shown.

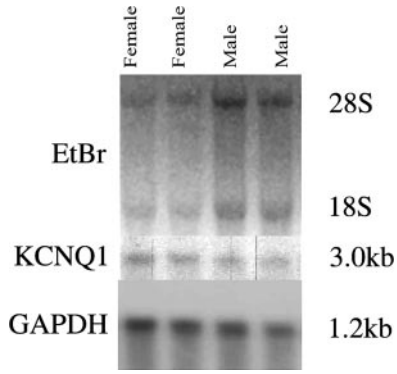

Fig. 2. Northern analysis revealing transcripts at ~3.0 kb, an appropriate size for KCNQ1 mRNA, in mRNA isolated from whole kidneys of 2 male and 2 female mice. Ethidium bromide (EtBr) staining and Northern blots for GAPDH were used as loading controls.

min in the presence of transfer buffer [10 mM 3-cyclohexylamino-1-propanesulfonic acid (pH 11.0) and 10% methanol] packed in ice. The membrane was blocked for 1 h in 5% nonfat dry milk and then cross-reacted for 1 h with the anti-KCNQ1 antibody (catalog no. H-130, Santa Cruz Biotechnology, Santa Cruz, CA) at a 1:200 dilution dissolved in antibody buffer (50 mM NaH_2PO_4, 150 mM NaCl, 0.1% Tween 20, and 3% BSA). The membrane was washed with PBST (50 mM NaH_2PO_4, 150 mM NaCl, and 0.1% Tween 20), incubated for 1 h with horseradish peroxidase-conjugated goat anti-rabbit IgG (ICN, Irvine, CA), detected using the enhanced chemiluminescence detection reagents (Amersham), and exposed to Hyperfilm ECL (Amersham).

Primary Antibodies

Anti-KCNQ1 is a rabbit polyclonal antibody that recognizes amino acids 547–676 mapping at the carboxy terminus of KCNQ1 of human origin (Santa Cruz Biotechnology).

Anti-anion exchanger 1 (AE1) is a rabbit polyclonal antibody raised against a 20-amino acid peptide from the amino terminus of rat AE1 (Alpha Diagnostic International, San Antonio, TX). This antibody localizes to the basolateral region of medullary intercalated cells and type A intercalated cells in the CCD, initial collecting tubule (ICT), and CNT (31, 36).

Anti-pendrin is a polyclonal antibody raised in rabbit that recognizes amino acids 766–780 of the human pendrin protein sequence. It localizes exclusively in the apical region of non-A intercalated cells in collecting duct and CNT (35, 40).

Anti-thiazide-sensitive Na^+-Cl^- cotransporter (TSC) is a polyclonal antibody (provided by Dr. Steven C. Hebert, Harvard University) raised in rabbit against a 110-amino acid segment of the amino terminus of rTSC1, which corresponds to amino acids 2–112 of the rat rTSC1. It has been characterized and localizes exclusively in the apical region of DCT cells (25, 39).

Anti-RhBG is a polyclonal antibody raised in rabbit against a 16-amino acid peptide in the cytoplasmic region near the carboxy terminus of mouse RhBG. It has been characterized and localizes in the basolateral region of all CCD and CNT cells, with the exception of type B intercalated cells (37).

Tissue Preparation for Immunohistochemical Localization of KCNQ1

Mice were anesthetized with intraperitoneal pentobarbital sodium or inhalant isoflurane. The kidneys and stomachs were preserved by in vivo cardiac perfusion with PBS (pH 7.4) and then with 2% paraformaldehyde-lysine-periodate followed by immersion in fixative overnight at 4°C. For light microscopy, transverse slices of kidney and stomach from each animal were embedded in polyester wax (polyethylene glycol 400 distearate, Polysciences, Warrington, PA). Sections (2–3 μm thick) were mounted on gelatin-coated glass slides.

Immunohistochemistry

Localization of KCNQ1 was accomplished using immunoperoxidase procedures. In initial experiments, the sections were dewaxed in ethanol, rehydrated, and then rinsed in PBS. The sections were incubated in 3% H_2O_2 in water for 30 min to block endogenous peroxidase activity, rinsed with PBS, treated for 15 min with 5% normal goat serum (NGS) in PBS, and then incubated at 4°C overnight with the anti-KCNQ1 antibody diluted 1:100 in PBS (kidney) and 1:1,000 in PBS (stomach). The sections were then washed in PBS, incubated for 30 min with biotinylated goat anti-rabbit IgG secondary antibody (Jackson ImmunoResearch, West Grove, PA) diluted 1:250 in PBS, and washed with PBS. The sections were treated for 30 min with the avidin-biotin complex reagent, rinsed with PBS, and then exposed to diaminobenzidine. The sections were washed in distilled water and dehydrated with xylene, mounted using Permount (Fisher Scientific, Fair Lawn, NJ), and observed by light microscopy.

In later experiments, immunohistochemical experiments were performed as described above with the following exceptions: for protein blocking, the section was exposed to 10% NGS for 30 min and then to Mouse Detective (Biocare Medical, Concord, CA) for 45 min; the anti-KCNQ1 antibody was diluted 1:500 in PBS with 5% NGS; and the secondary antibody was a polymer-linked peroxidase-conjugated goat anti-rabbit IgG (MACH2, Biocare Medical, Walnut Creek, CA). For this procedure, the avidin-biotin-peroxidase complex reagent was unnecessary and, thus, was omitted.

Antigen retrieval methods were also applied to determine whether additional immunoreactivity could be detected. Dewaxed sections were heated in a microwave oven to 100°C in citrate buffer for 10 min or in Trilogy (Cell Marque, Hot Springs, AR) for 5 min, cooled to room temperature, and rinsed in PBS before the peroxidase blocking step.

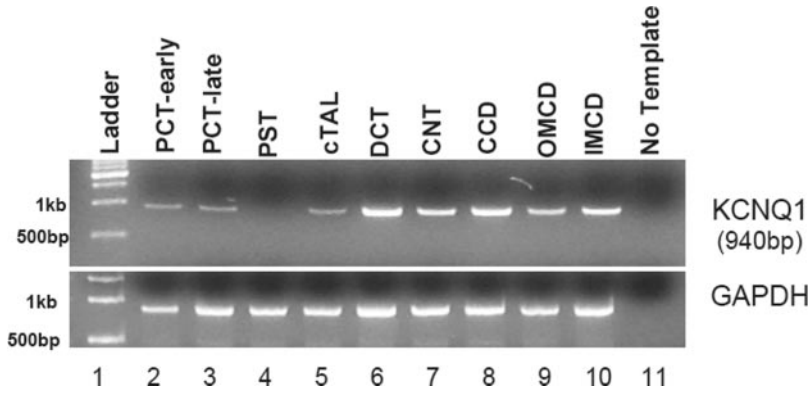

Fig. 3. RT-PCR of isolated tubule segments using primers to 940 bp of the coding region of KCNQ1 (accession no. BC055304). KCNQ1 mRNA expression was detected in all collecting duct segments, distal convoluted tubule (DCT), connecting segment (CNT), and cortical thick ascending limb (cTAL). The cortical proximal straight tubule (PST) was consistently negative, whereas signal in the late proximal convoluted tubule (PCT-late) consistently gave a weak signal. Signal was detected inconsistently from the early PCT. Controls with RT omitted were run for every segment and produced no signal. Controls with template omitted were run for both KCNQ1 and GAPDH reactions and also produced no signal.

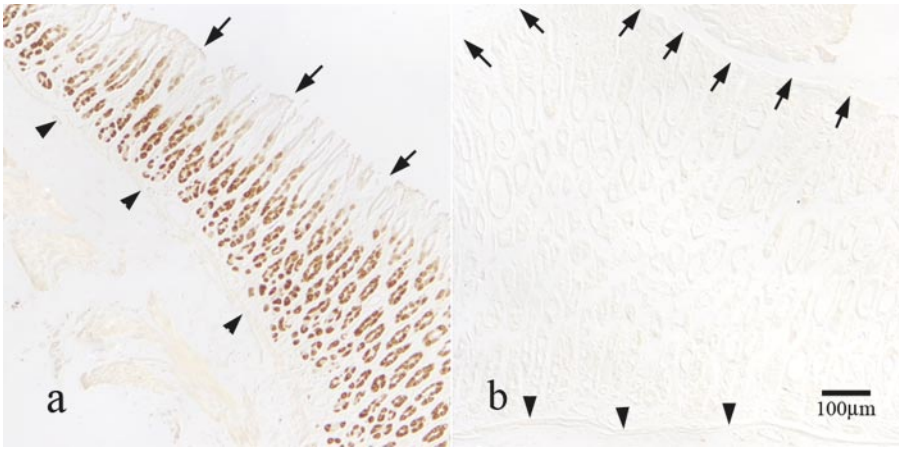

Fig. 4. Immunohistochemical localization of KCNQ1 in mouse stomach. Intense KCNQ1 immunoreactivity is present in parietal cells in C3H/HeJCrl-Kcnq1 wild-type mouse stomach (*a*). No immunoreactivity is present in C3H/HeJCrl-Kcnq1$^{vtg\text{-}2J}$/J mutant mouse stomach (*b*). Gastric mucosa is markedly hypertrophied in C3H/HeJCrl-Kcnq1$^{vtg\text{-}2J}$/J mutant mouse stomach; compare span between arrows at luminal surface and arrowheads at muscularis mucosa in *a* and *b*.

Double Labeling for KCNQ1 With TSC, AE1, Pendrin, and RhBG Immunoreactivity

Double labeling was accomplished using sequential immunoperoxidase procedures. Kidney sections were dewaxed in ethanol, rehydrated, and then rinsed in PBS. Endogenous peroxidase activity was blocked by incubation of the sections in 3% H_2O_2 in water for 30 min. In experiments using the avidin-biotin-peroxidase method, the sections were rinsed in PBS, treated for 15 min with 5% NGS in PBS, and then incubated at 4°C overnight with anti-KCNQ1 antibody diluted 1:100 in PBS. The sections were washed in PBS, incubated for 30 min with the biotinylated goat anti-rabbit IgG secondary antibody diluted 1:250 in PBS, and then washed with PBS. The sections were treated for 30 min with the avidin-biotin complex reagent, rinsed with PBS, and then exposed to diaminobenzidine. The sections were washed in glass-distilled water and then in PBS and incubated in 3% H_2O_2 in water for 30 min. The sections were again washed in PBS and incubated for 15 min with 5% NGS in PBS. The sections were treated

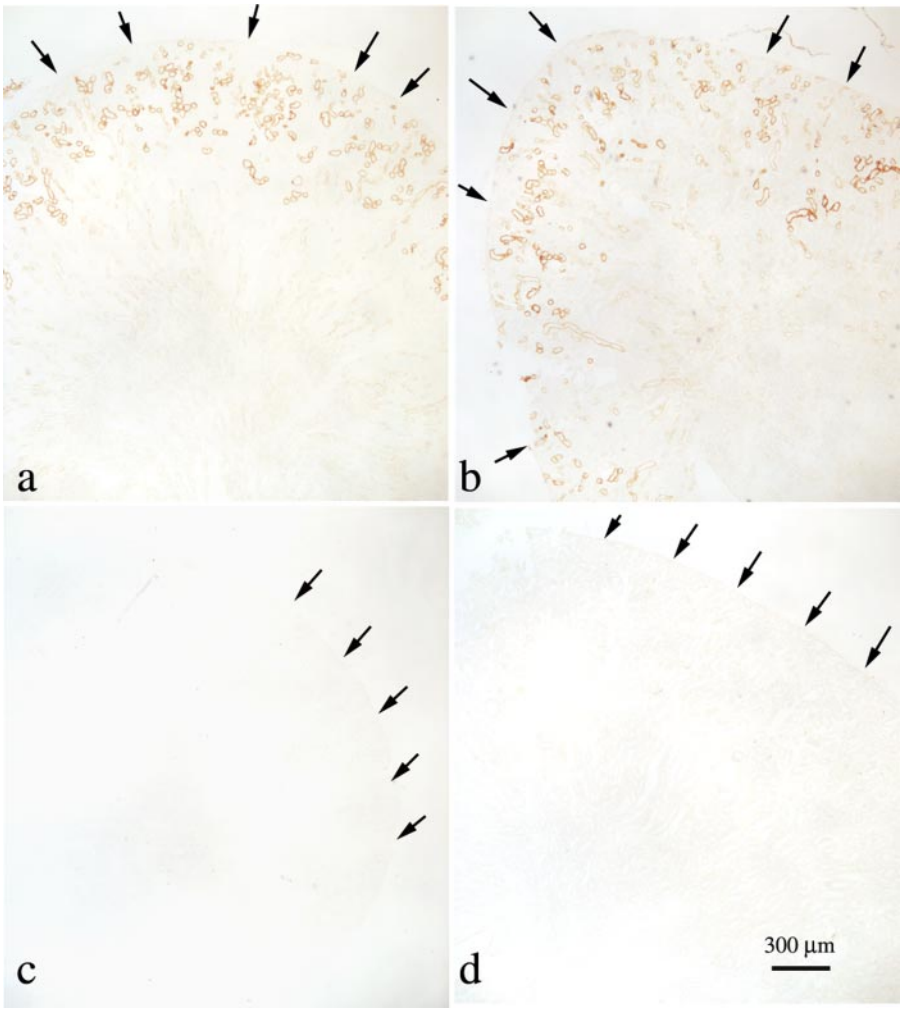

Fig. 5. Low-magnification images of KCNQ1 immunoreactivity in mouse kidney. In normal mice [C57BL/6 mouse (*a*) and C3H/HeJCrl-Kcnq1 wild-type mouse (*b*)], intense KCNQ1 immunoreactivity is present in a minority of tubules in the renal cortex. In C3H/HeJCrl-Kcnq1 wild-type mouse kidney treated with no primary antibody (*c*) and C3H/HeJCrl-Kcnq1$^{vtg\text{-}2J}$/J mutant mouse kidney (*d*), there was no immunoreactivity. Arrows, renal capsule.

overnight with the second primary antibody diluted in PBS: anti-TSC diluted 1:8,000, anti-AE1 diluted 1:800, and anti-pendrin diluted 1:1,000 were used in separate experiments. The sections were washed in PBS and incubated for 30 min with the biotinylated goat anti-rabbit IgG secondary antibody. The sections were washed with PBS, incubated with the avidin-biotin complex reagent, and washed with PBS. For detection of the second immunoreaction, Vector SG (Vector Laboratories, Burlingame, CA) was used as the chromogen to produce a blue label, which was easily distinguishable from the brown label produced by the diaminobenzidine used for detection of KCNQ1 immunoreactivity. The sections were washed with glass-distilled water, dehydrated with xylene, mounted using Permount, and observed by light microscopy. Additional double-labeling experiments were done using the anti-KCNQ1 antibody diluted 1:500 with anti-AE1 diluted 1:800 or anti-RhBG diluted 1:1,000 and using the polymer-linked peroxidase-conjugated secondary antibody for detection, instead of the avidin-biotin-peroxidase method.

Sections were photographed using a Nikon LaboPhot-2 microscope equipped with a 35-mm film camera or a Nikon E600 microscope equipped with differential interference contrast optics and photographed using a DXM1200F digital camera and ACT-1 software (Nikon).

Identification of Tubule Segments and Specific Epithelial Cell Types

Individual tubule segments were identified by morphological criteria and colocalization with specific epithelial cell antigens. The results of the double-labeling experiments with antigens specific for particular cells were used to definitively identify individual cell types (see *Primary Antibodies*).

The DCT was identified using apical TSC immunoreactivity. Late portions of the DCT were identified definitively by transitions from DCT to CNT; the early DCT was identified by transitions from the cTAL to the DCT.

The CNT was identified by its location in the cortical labyrinth, its characteristic tall cuboidal cells with irregular luminal profiles and cellular heterogeneity, and transitions from the DCT or to the lower-profile ICT.

The ICT and CCD were identified by their characteristic cellular heterogeneity: the ICT has a lower profile than the CNT. The ICT and CCD were distinguished from each other by their locations in the cortical labyrinth and in the medullary ray, respectively.

Controls

For controls in each immunolocalization procedure, PBS was substituted for the primary antibody. For double-labeling procedures, controls in each experiment included substitution of PBS only for the first primary antibody, the second primary antibody, and both primary antibodies. Additionally, sections of kidney and stomach from phenotypically mutant C3H/HeJCrl-Kcnq1$^{vtg\text{-}2J}$/J mice were studied in single-labeling experiments in which the anti-KCNQ1 antibodies were used to verify that the antibodies detected only KCNQ1 protein.

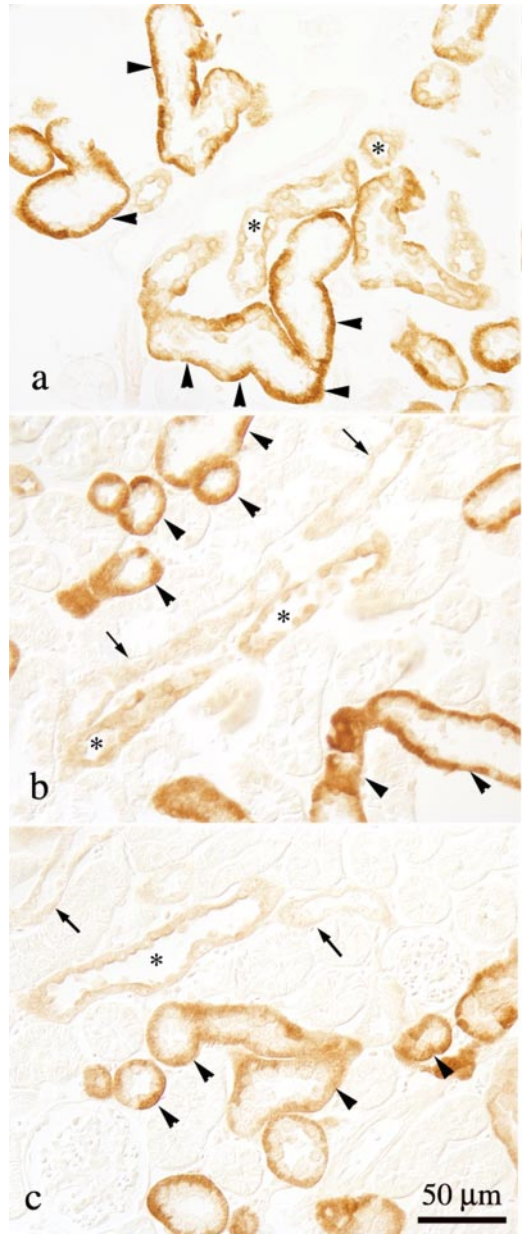

Fig. 6. Immunohistochemical detection of KCNQ1 immunoreactivity with and without antigen retrieval procedures in mouse renal cortex. *a*: Routine detection method using polymer-linked peroxidase-conjugated secondary antibody. *b*: Procedure described in *a* after antigen retrieval using citrate buffer. *c*: Procedure described in *a* after antigen retrieval using Trilogy. Labeling pattern is similar in all protocols. Prominent immunostaining is intense basolateral label in the DCT and CNT (arrowheads); weak apical staining is evident in the initial collecting tubule (ICT) and CCD (*); faint staining is present in the thick ascending limb (TAL, arrows); proximal tubules were negative.

RESULTS

Immunoblot Analysis

Immunoblots of membrane protein isolated from kidney and stomach detected KCNQ1 immunoreactivity at ~75 kDa, the expected mobility for KCNQ1 (Fig. 1).

Northern Analysis and RT-PCR

Northern analysis revealed transcripts in whole kidney (n = 4) of ~3.0 kb, an appropriate size for KCNQ1 mRNA (Fig. 2). RT-PCR of isolated tubule segments detected KCNQ1 mRNA expression in glomeruli (not shown), DCT, CNT, and all collecting duct segments, including CCD, OMCD, and IMCD (Fig. 3). Expression was also detected in cTAL segments, although the signal was weak. No signal was detected in proximal straight tubules, but a weak signal was detected consistently in late proximal convoluted tubules (Fig. 3). In early proximal convoluted tubules, KCNQ1 mRNA was detected inconsistently. No signal was detected in the absence of RT or cDNA template.

Immunolocalization of KCNQ1

General observations. In the stomach, KCNQ1 immunoreactivity was consistent with previous reports demonstrating its presence in gastric parietal cells (Fig. 4). Stomachs from the KCNQ1 mutant phenotype mice were negative (Fig. 4). KCNQ1 immunoreactivity was distributed throughout the renal cortex (Fig. 5) in the DCT, CNT, ICT, and CCD (Figs. 6 and 7). Proximal tubules were consistently negative for KCNQ1 (Figs. 6 and 7). Intense basolateral KCNQ1 immunostaining was observed in the DCT and CNT (Fig. *7, a–d*). In the CCD and ICT, the majority of cells exhibited KCNQ1 immunoreactivity, but labeling intensity was weaker than in the CNT and DCT. In the CCD and ICT, a few cells showed intense apical immunoreactivity, whereas the majority of cells exhibited diffuse apical or cytoplasmic staining (Figs. 7, *e–h*). In the OMCD, KCNQ1 immunolabel was weak and diffuse. In the initial IMCD, KCNQ1 labeling was observed in the basolateral region of the majority cell type, with the morphological appearance of principal cells. Diffuse label was observed in

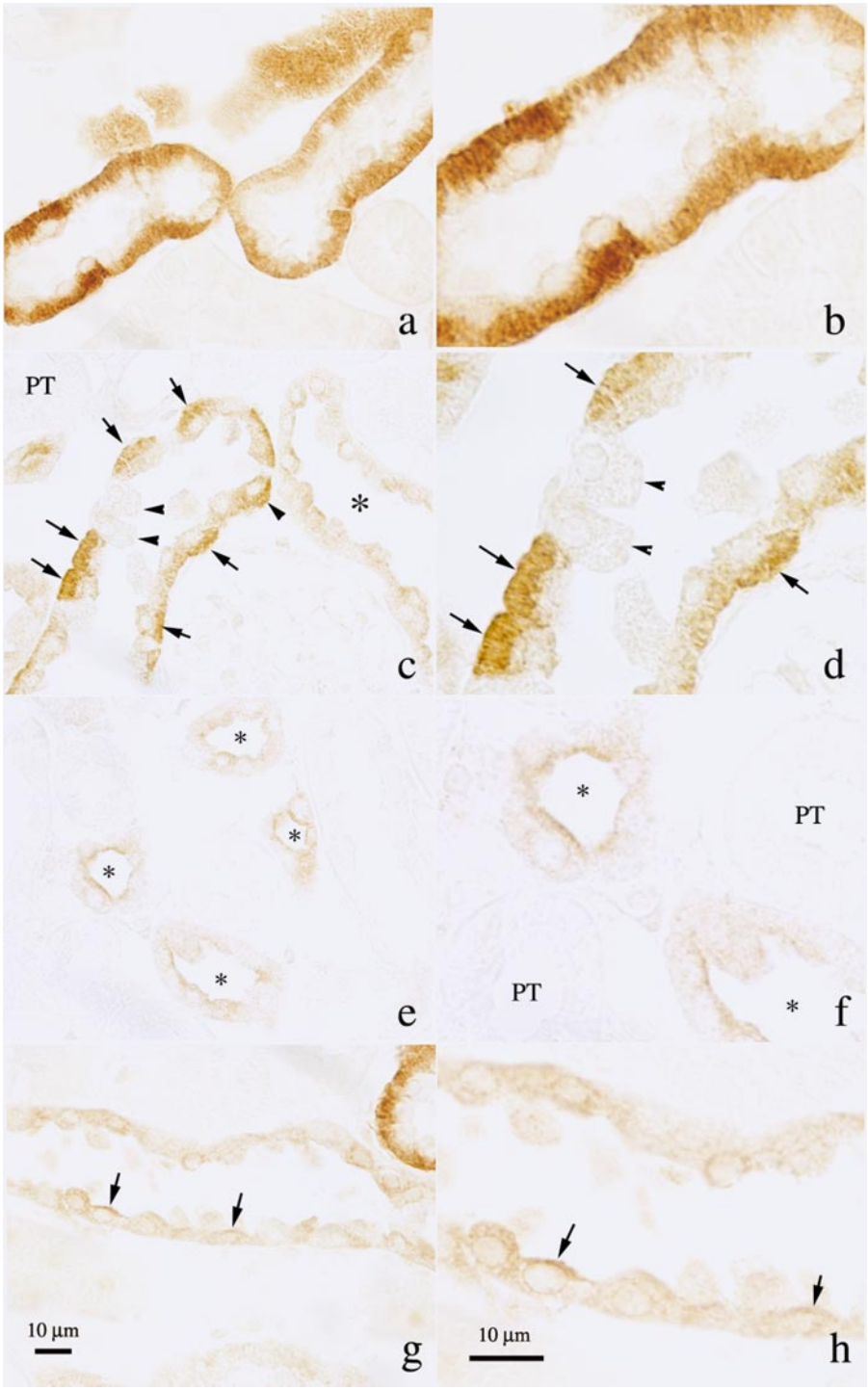

Fig. 7. Higher-magnification images of tubule segments expressing KCNQ1 immunoreactivity in renal cortex. In the DCT (*a* and *b*), virtually all cells exhibited basolateral immunoreactivity, although the intensity of immunolabel varied among the DCT profiles. In the CNT (*c* and *d*), the majority of cells (connecting tubule cells) exhibited intense basolateral immunoreactivity that extended deep into the cells (arrows). In a subpopulation of cells, no immunoreactivity was detectable (arrowheads). The apical surface of negative cells typically bulged into the tubule lumen, and the nuclei of these cells were more basal than those of CNT cells, suggesting that they were non-A, non-B intercalated cells. Only rare cells in the CNT had apical KCNQ1 immunostaining (not shown). In contrast, ICT (*e* and *f*; ∗ in *c*) typically exhibited apical staining in the majority of cells. The apical staining was less intense than basolateral staining observed in the DCT and CNT. In the CCD (*g* and *h*), immunostaining was typically diffuse, although individual cells exhibited discrete apical immunoreactivity (arrows). Proximal tubules (*c* and *f*, PT) were consistently negative for KCNQ1 immunoreactivity. Scale bar in *g* also applies to *a, c,* and *e*; scale bar in *h* also applies to *b, d,* and *f*.

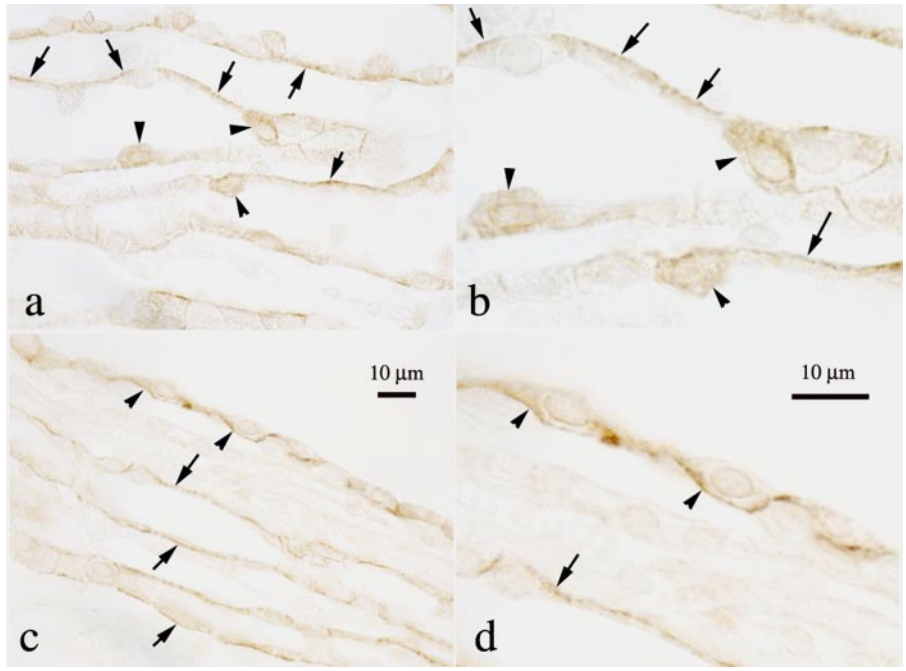

Fig. 8. Immunohistochemical localization of KCNQ1 immunoreactivity in the IMCD (*a* and *b*) and surface papillary epithelium (*c* and *d*). Distinct KCNQ1 immunolabel was evident in the IMCD from the border with the outer medulla and extending through approximately the proximal third of the papillary IMCD. *a* and *b*: IMCD in the upper portion of the papilla; basolateral immunolabel was present in principal cells (arrows), whereas label in intercalated cells was diffuse (arrowheads). *c* and *d*: Basolateral KCNQ1 immunolabel in surface papillary epithelial cells (arrowheads) and basolateral labeling in principal cells in IMCD (arrows). Scale bar in *c* also applies to *a*; scale bar in *d* also applies to *b*.

intercalated cells in this segment (Fig. 8). However, in terminal IMCD, KCNQ1 immunoreactivity was weak or absent. The papillary surface epithelium has strong basolateral label in a subpopulation of cells (Fig. 8, *c* and *d*). Weak basolateral immunostaining was also observed in the medullary TAL and cTAL (Figs. 6 and 9, *a* and *b*). Endothelial label was frequently detected in arterioles (Fig. 9*c*).

The pattern of immunoreactivity in wild-type mice for the KCNQ1 gene was consistent, regardless of the mouse strain (Fig. 5, *a* and *b*). No KCNQ1 labeling was observed in kidney sections from KCNQ1 mutant mice (Fig. 5*d*). Moreover, labeling was not observed in sections from normal mouse kidney when the primary antibody was omitted (Fig. 5*c*). Proximal tubules were negative for KCNQ1 staining in all experiments, including experiments in which two different methods of antigen retrieval were used (Fig. 6).

Detailed observations. Double-labeling sections for KCNQ1 and TSC specifically identified DCT cells and demonstrated axial heterogeneity of KCNQ1 expression within the DCT (Fig. 10*a*). In the late DCT, we observed strong basolateral KCNQ1 immunoreactivity in the majority of cells. In the early DCT, most cells exhibited relatively weak basolateral label.

In the CNT, nearly all cells exhibited strong basolateral KCNQ1 immunoreactivity (Fig. 7, *c* and *d*). A minority of cells showed no detectable immunoreactivity; these cells typically bulged into the tubule lumen and had basal nuclei, consistent with the appearance of non-A, non-B intercalated cells, which are common in the CNT. Occasional cells had apical immunolabel, but no basolateral immunostaining.

In the ICT, the distribution of KCNQ1 immunoreactivity was heterogeneous. Moderate-intensity basolateral KCNQ1 immunoreactivity was observed in a few cells, particularly near the transition from the CNT. However, the majority of cells in the ICT typically exhibited diffuse apical immunolabel, but no basolateral label, and a subpopulation of cells showed intense, discrete apical immunoreactivity (Fig. 7, *e* and *f*).

In the CCD, the KCNQ1 immunolabel was heterogeneous. In the majority of cells, immunostaining was weak and diffuse. However, a subpopulation of cells in the CCD exhibited intense and discretely apical KCNQ1 immunolabel. The majority of cells did not exhibit basolateral immunoreactivity, and a subpopulation of cells showed no detectable immunostaining (Fig. 7, *g* and *h*).

Colocalization of KCNQ1 immunoreactivity with markers for specific epithelial cell types was done to identify the cells in the CNT, ICT, and CCD that exhibited no KCNQ1 immunolabel or apical KCNQ1. A double-labeling experiment with pendrin showed no detectable basolateral KCNQ1 immunoreactivity in type B and non-A, non-B intercalated cells (Fig. 10, *b* and *c*). Furthermore, pendrin-positive intercalated cells showed no apical KCNQ1 immunoreactivity (Fig. 10*b*). However, intense pendrin immunoreactivity in the apical region of intercalated cells in the CCD and ICT may have obscured apical KCNQ1 immunoreactivity.

RhBG, an ammonia transport protein, is abundant in the basolateral plasma membrane of all cells in the CNT, ICT, and CCD, except type B intercalated cells. In the type B intercalated cell, RhBG immunoreactivity is undetectable (37). Double-labeling experiments using anti-KCNQ1 and anti-RhBG antibodies demonstrated apical KCNQ1 immunoreactivity in cells with no RhBG immunoreactivity, which indicates that type B intercalated cells express apical KCNQ1 (Fig. 11*e*). Other cells exhibited basolateral RhBG and apical KCNQ1 immunoreactivity, and the majority of these cells had the appearance of principal cells (Fig. 11*e*). Intercalated cells in the CNT with basolateral RhBG and the morphological features of non-A, non-B intercalated cells exhibited no KCNQ1 immunoreactivity (Fig. 11*d*). These data indicate that principal cells and type B intercalated cells in the ICT and CCD express apical KCNQ1.

Double-labeling experiments for AE1, which identifies type A intercalated cells, revealed no detectable KCNQ1 immuno-

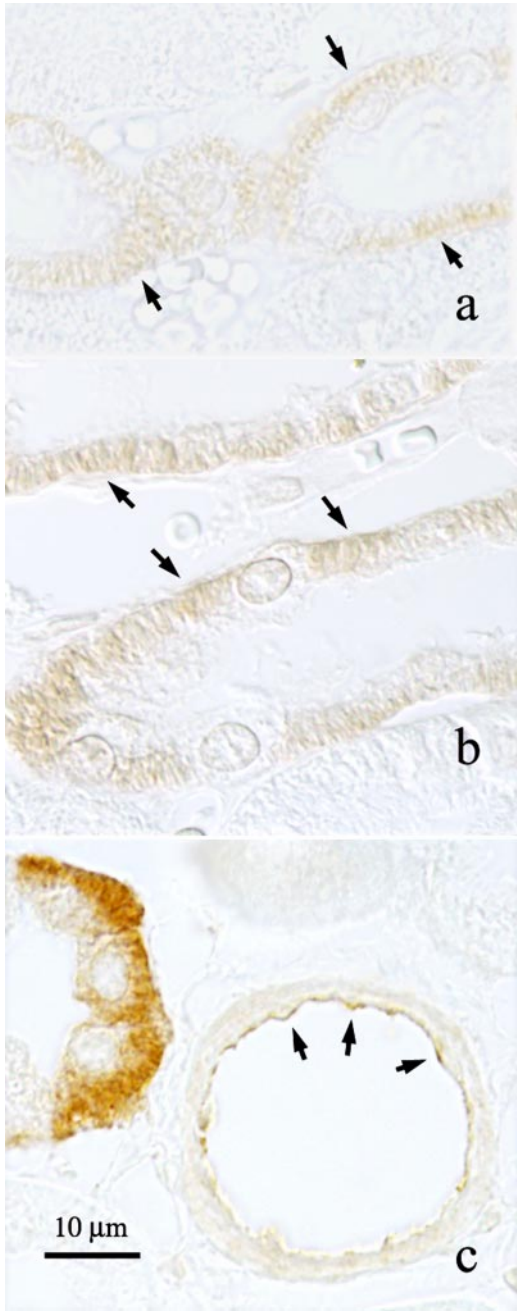

Fig. 9. Immunohistochemical localization of KCNQ1 in thick ascending limbs (TAL) and vascular endothelium. In cortical (*a*) and medullary (*b*) TAL, weak basolateral KCNQ1 immunoreactivity was consistently detected (arrows). KCNQ1 immunoreactivity could be detected frequently lining renal arterioles, consistent with immunostaining of endothelial cells (*c*, arrows).

reactivity in the majority of type A intercalated cells, although some type A intercalated cells exhibited diffuse apical KCNQ1 immunoreactivity (Fig. 11, *a–c*). We did not observe AE1-positive cells with detectable basolateral KCNQ1 immunoreactivity. Thus basolateral KCNQ1 in the CNT and ICT appears to be located in the CNT cells and principal cells, and the majority of type A intercalated cells in the CCD and ICT have no convincing KCNQ1 signal. However, apical KCNQ1 immunoreactivity can be detected in a few type A intercalated cells.

In the OMCD in the outer stripe, faint and primarily diffuse KCNQ1 immunolabel was observed; in the OMCD in the inner stripe immunostaining was primarily weak and diffuse, although basolateral immunoreactivity was observed in occasional principal cells. Moreover, cytoplasmic staining was intensified in the apical region of some intercalated cells.

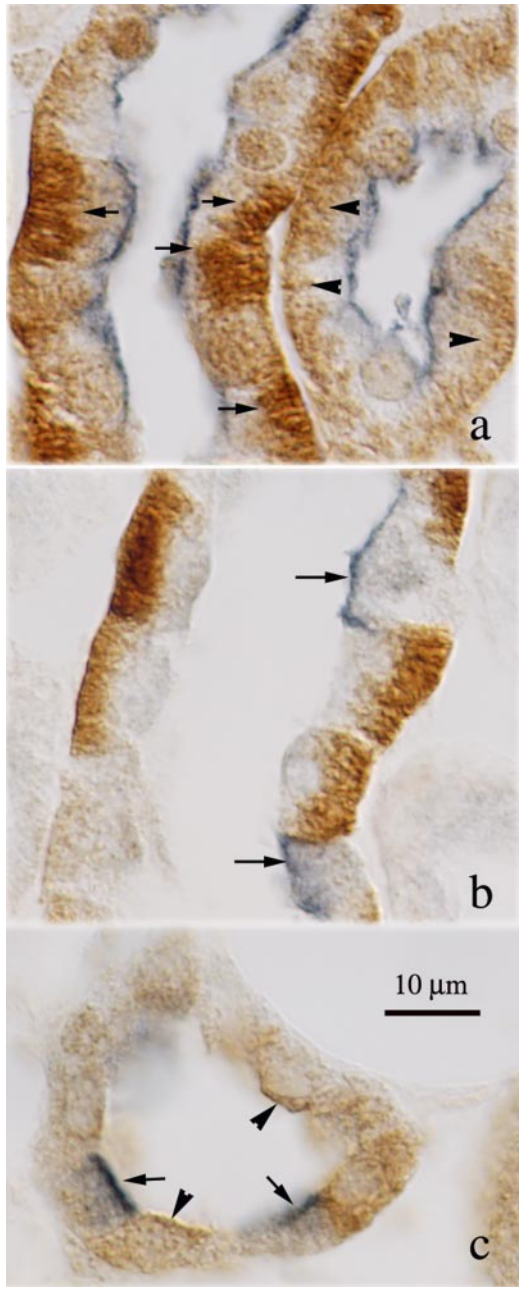

Fig. 10. Immunohistochemical double labeling for KCNQ1 (brown reaction product) and markers for specific epithelial cells (blue reaction product). *a*: Thiazide-sensitive NaCl cotransporter (TSC). *b* and *c*: Apical Cl^-/HCO_3^- exchanger pendrin. Double-labeling experiments for KCNQ1 and TSC demonstrate basolateral KCNQ1 immunoreactivity that varies in intensity in DCT cells (*a*). Late DCT exhibits intense basolateral KCNQ1 immunoreactivity in the majority of cells (arrows); basolateral KCNQ1 immunoreactivity was weaker in early DCT (arrowheads). KCNQ1 and pendrin double-labeling experiments demonstrate no basolateral KCNQ1 immunolabel of non-A intercalated cells (arrows, *b* and *c*). Pendrin-negative cells in the ICT (type A intercalated cells or principal cells) exhibit apical KCNQ1 immunoreactivity (arrowheads, *c*).

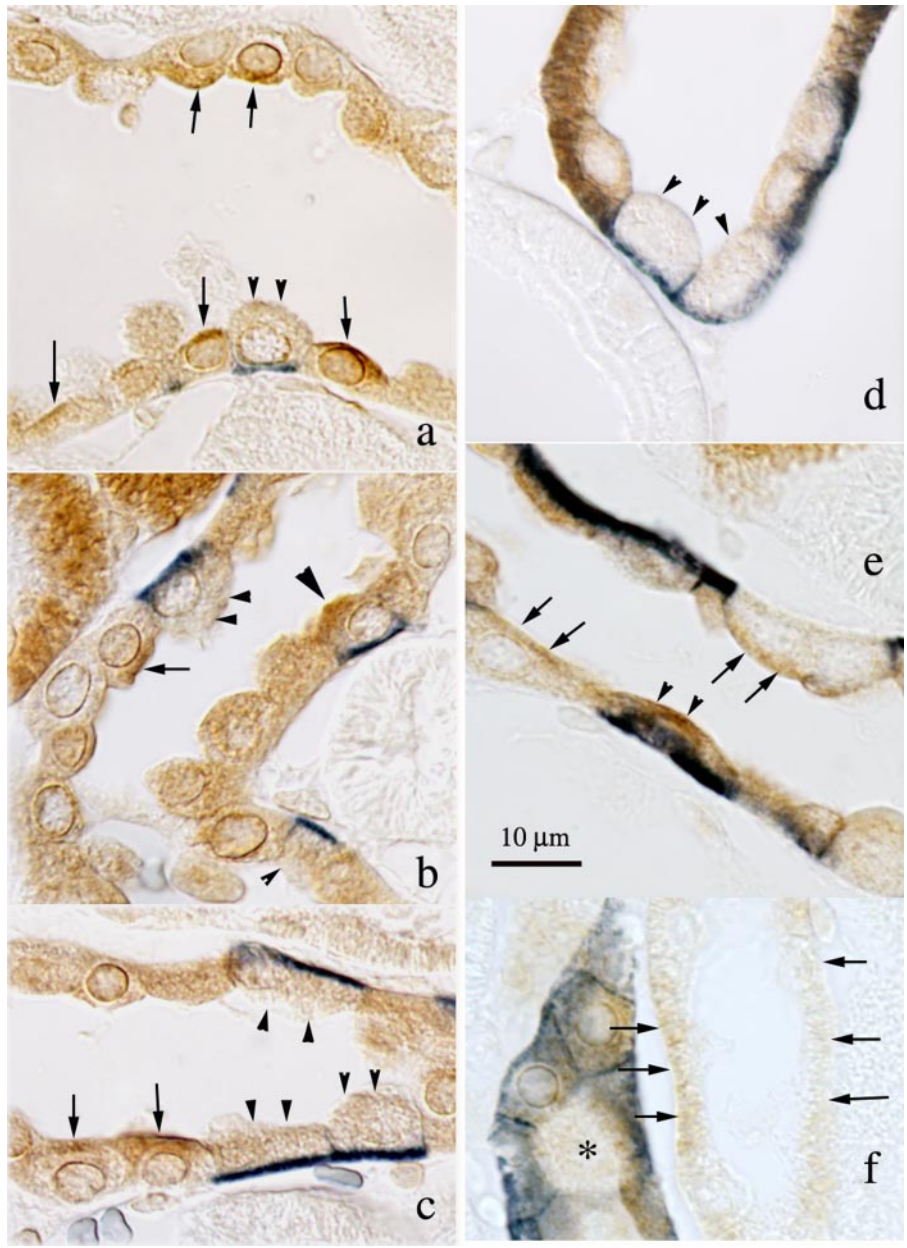

Fig. 11. Immunohistochemical double labeling for KCNQ1 (brown reaction product) and markers for specific epithelial cells (blue reaction product). *a–c*: Anion exchanger 1 (AE1). *d–f*: Ammonium transporter RhBG. KCNQ1 and AE1 double labeling demonstrated that the majority of cells in the ICT and CCD that exhibited discrete apical KCNQ1 immunoreactivity (arrows) were AE1 negative, i.e., principal cells or non-A intercalated cells. AE1-positive cells typically did not exhibit apical KCNQ1 label (small arrowheads), although a few AE1-positive cells did exhibit apical KCNQ1 immunoreactivity (large arrowhead, *b*). RhBG-positive intercalated cells in the CNT with the profile of non-A, non-B intercalated cells were negative for KCNQ1 (*d*, arrowheads). KCNQ1 and RhBG double labeling demonstrated that RhBG-negative cells in the ICT, i.e., type B intercalated cells, frequently expressed apical KCNQ1 (*e*, arrows); principal cells also expressed apical KCNQ1 (*e*, arrowheads). Weak KCNQ1 immunoreactivity was detected in the basolateral region of the TAL (*f*, arrows). Adjacent CCD is strongly labeled for RhBG (*).

In the initial IMCD (Fig. 8), the majority of cells, which had the appearance of principal cells, exhibited discrete immunolabel along the basolateral region. Cells with the appearance of intercalated cells generally exhibited diffuse cytoplasmic staining.

DISCUSSION

Using Northern analysis, RT-PCR, and Western analysis, we have confirmed expression of KCNQ1 in the mouse kidney. RT-PCR demonstrated expression of the KCNQ1 gene in all collecting duct segments, cTAL, DCT, CNT, and glomeruli. No signal was detected in proximal straight tubules, although weak expression was detected in proximal convoluted tubules.

Immunohistochemical localization revealed heterogeneous distribution of KCNQ1, not only with respect to cell type, but also in its subcellular distribution. KCNQ1 immunoreactivity in the kidney was most intense in the late DCT and CNT, where its distribution was primarily basolateral. In the ICT and CCD, the majority of cells exhibited diffuse apical KCNQ1 immunoreactivity, although cells with discrete apical immunoreactivity were frequently observed. Basolateral labeling was also present in a minority of cells in the ICT near the transition from the CNT. In the IMCD, principal cells exhibited basolateral KCNQ1 immunoreactivity and intercalated cells appeared to have diffuse staining. These observations suggest that KCNQ1 serves cell-specific roles in renal K^+ transport.

In the stomach, acid secretion is accomplished by parietal cells via apical H^+-K^+-ATPase. Recent studies have demonstrated that KCNQ1 is also present in parietal cells (13), which was confirmed here, and is necessary for gastric acid secretion (10, 34). Isoforms of H^+-K^+-ATPase are present in intercalated cells and principal cells of the mammalian collecting duct

(1, 2, 28, 38, 43) and contribute to acid secretion, similar to the gastric parietal cell (44). The cooperation of an apical K^+ channel with H^+-K^+-ATPase transport has been proposed in previous studies from our laboratory (44, 46). Under K^+-replete conditions, apical H^+-K^+-ATPase transport in the rabbit CCD is accompanied by apical K^+ recycling, resulting in proton secretion without transepithelial K^+ absorption (44, 46). Whether KCNQ1 participates in this process in the collecting duct remains to be determined.

Our data indicate that principal cells in the ICT and CCD express apical KCNQ1. The ROMK channel is present at the apical membrane of these segments and is thought to be a major mechanism for K^+ secretion. However, ROMK-knockout mice are able to secrete K^+ without developing hyperkalemia (21, 22); thus other pathways for K^+ secretion exist (12). Apical KCNQ1 in the ICT and CCD may serve this function.

In segments where basolateral KCNQ1 predominates, that is, the TAL, DCT, CNT, and IMCD, KCNQ1 should participate in K^+ extrusion across the basolateral plasma membrane because of the electrochemical gradient for K^+ from the cell to the extracellular space. Otherwise, the function of basolateral KCNQ1 in these cells is unknown. Other investigators have reported basolateral KCNQ1 in Madin-Darby canine kidney cells, but its function here is unknown as well (14). In mouse tracheal and colonic epithelia, basolateral KCNQ1 forms cAMP-responsive K^+ channels that facilitate Cl^- secretion by recycling intracellular K^+ and, thus, permitting a favorable electrochemical gradient for Cl^- uptake via a basolateral Na^+-K^+-$2Cl^-$ cotransporter (11, 23). Basolateral KCNQ1 may have a similar role in renal IMCD cells, where Cl^- secretion occurs (45). Basolateral KCNQ1 may also be involved in K^+ reabsorption, which also occurs in the IMCD (3). How basolateral KCNQ1 contributes to epithelial ion transport in distinct segments of the renal tubule remains to be determined.

In contrast to the results of other investigators (33, 34), we found no immunohistochemical evidence of KCNQ1 expression in the proximal tubule; however, using RT-PCR, we detected a weak signal in microdissected proximal convoluted tubules. The previous studies used antibodies directed against a peptide from the amino terminus of KCNQ1 and found distinct KCNQ1 immunoreactivity in the proximal convoluted and proximal straight tubule brush border by immunofluorescence, but no signal in distal tubules or collecting ducts (33). The antibodies and probes used in our experiments correspond to the carboxy terminus of KCNQ1 protein, as did the probe used for in situ hybridization, which also demonstrated KCNQ1 signal in distal tubules and collecting ducts (7). One possible explanation for these discrepant findings is the existence of different KCNQ1 isoforms in the mouse kidney.

In summary, KCNQ1 is expressed in a heterogeneous pattern in the TAL, DCT, CNT, ICT, and collecting duct. KCNQ1 may contribute to K^+ secretion or absorption, depending on its cellular distribution. Alternatively, KCNQ1 may participate in K^+ recycling, which facilitates transepithelial transport of another ion such as Cl^-. The distribution of KCNQ1 in renal tubules suggests a complex role for this K^+ channel in epithelial ion transport (18, 24, 26, 30, 42, 47).

ACKNOWLEDGMENTS

The authors gratefully acknowledge the invaluable assistance of the staff of the University of Florida College of Medicine Electron Microscope Core Facility, particularly Karen Chamusco and Jeanice Jaroll, Dr. Shen-Ling Xia for review of the manuscript, and Alicia Rudin for expert technical assistance.

Portions of this work were presented at the 37th Annual Meeting of the American Society of Nephrology (2004) and have been published in abstract form.

GRANTS

This work was supported by the Medical Research Service of the Department of Veterans Affairs and National Institute of Diabetes and Digestive and Kidney Diseases Grant RO1-DK-49750.

REFERENCES

1. **Ahn KY, Kone BC.** Expression and cellular localization of mRNA encoding the "gastric" isoform of H^+-K^+-ATPase α-subunit in rat kidney. *Am J Physiol Renal Fluid Electrolyte Physiol* 268: F99–F109, 1995.
2. **Ahn KY, Park KY, Kim KK, Kone BC.** Chronic hypokalemia enhances expression of the H^+-K^+-ATPase α_2-subunit gene in renal medulla. *Am J Physiol Renal Fluid Electrolyte Physiol* 271: F314–F321, 1996.
3. **Arrascue JF, Dobyan DC, Jamison RL.** Potassium recycling in the renal medulla: effects of acute potassium chloride administration to rats fed a potassium-free diet. *Kidney Int* 20: 348–352, 1981.
4. **Bleich M, Warth R.** The very small-conductance K^+ channel KvLQT1 and epithelial function. *Pflügers Arch* 440: 202–206, 2000.
5. **Casimiro MC, Knollmann BC, Yamoah EN, Nie L, Vary JC Jr, Sirenko SG, Greene AE, Grinberg A, Huang SP, Ebert SN, Pfeifer K.** Targeted point mutagenesis of mouse Kcnq1: phenotypic analysis of mice with point mutations that cause Romano-Ward syndrome in humans. *Genomics* 84: 555–564, 2004.
6. **Chen Q, Zhang D, Gingell RL, Moss AJ, Napolitano C, Priori SG, Schwartz PJ, Kehoe E, Robinson JL, Schulze-Bahr E, Wang Q, Towbin JA.** Homozygous deletion in KVLQT1 associated with Jervell and Lange-Nielsen syndrome. *Circulation* 99: 1344–1347, 1999.
7. **Demolombe S, Franco D, de BP, Kuperschmidt S, Roden D, Pereon Y, Jarry A, Moorman AF, Escande D.** Differential expression of KvLQT1 and its regulator IsK in mouse epithelia. *Am J Physiol Cell Physiol* 280: C359–C372, 2001.
8. **Dilly KW, Kurokawa J, Terrenoire C, Reiken S, Lederer WJ, Marks AR, Kass RS.** Overexpression of β_2-adrenergic receptors cAMP-dependent protein kinase phosphorylates and modulates slow delayed rectifier potassium channels expressed in murine heart: evidence for receptor/channel co-localization. *J Biol Chem* 279: 40778–40787, 2004.
9. **Frank AE, Weiner ID.** Effects of ammonia on acid-base transport by the B-type intercalated cell. *J Am Soc Nephrol* 12: 1607–1614, 2001.
10. **Grahammer F, Herling AW, Lang HJ, Schmitt-Graff A, Wittekindt OH, Nitschke R, Bleich M, Barhanin J, Warth R.** The cardiac K^+ channel KCNQ1 is essential for gastric acid secretion. *Gastroenterology* 120: 1363–1371, 2001.
11. **Grahammer F, Warth R, Barhanin J, Bleich M, Hug MJ.** The small conductance K^+ channel, KCNQ1: expression, function, and subunit composition in murine trachea. *J Biol Chem* 276: 42268–42275, 2001.
12. **Gray DA, Frindt G, Palmer LG.** Quantification of K^+ secretion through apical low-conductance K channels in the CCD. *Am J Physiol Renal Physiol* 289: F117–F126, 2005.
13. **Heitzmann D, Grahammer F, von HT, Schmitt-Graff A, Romeo E, Nitschke R, Gerlach U, Lang HJ, Verrey F, Barhanin J, Warth R.** Heteromeric KCNE2/KCNQ1 potassium channels in the luminal membrane of gastric parietal cells. *J Physiol* 561: 547–557, 2004.
14. **Jespersen T, Rasmussen HB, Grunnet M, Jensen HS, Angelo K, Dupuis DS, Vogel LK, Jorgensen NK, Klaerke DA, Olesen SP.** Basolateral localisation of KCNQ1 potassium channels in MDCK cells: molecular identification of an N-terminal targeting motif. *J Cell Sci* 117: 4517–4526, 2004.
15. **Kaunitz JD, Gunther RD, Sachs G.** Characterization of an electrogenic ATP and chloride-dependent proton translocating pump from rat renal medulla. *J Biol Chem* 260: 11567–11573, 1985.
16. **Kim SJ, Greger R.** Voltage-dependent, slowly activating K^+ current (I_{Ks}) and its augmentation by carbachol in rat pancreatic acini. *Pflügers Arch* 438: 604–611, 1999.
17. **Kim SJ, Kim JK, Pavenstadt H, Greger R, Hug MJ, Bleich M.** Regulation of slowly activating potassium current (I_{Ks}) by secretin in rat pancreatic acinar cells. *J Physiol* 535: 349–358, 2001.
18. **Kurokawa J, Motoike HK, Rao J, Kass RS.** Regulatory actions of the A-kinase anchoring protein Yotiao on a heart potassium channel down-

stream of PKA phosphorylation. *Proc Natl Acad Sci USA* 101: 16374–16378, 2004.
19. **Lambrecht NW, Yakubov I, Scott D, Sachs G.** Identification of the K efflux channel coupled to the gastric H-K-ATPase during acid secretion. *Physiol Genomics* 21: 81–91, 2005.
20. **Lee MP, Ravenel JD, Hu RJ, Lustig LR, Tomaselli G, Berger RD, Brandenburg SA, Litzi TJ, Bunton TE, Limb C, Francis H, Gorelikow M, Gu H, Washington K, Argani P, Goldenring JR, Coffey RJ, Feinberg AP.** Targeted disruption of the Kvlqt1 gene causes deafness and gastric hyperplasia in mice. *J Clin Invest* 106: 1447–1455, 2000.
21. **Lorenz JN, Baird NR, Judd LM, Noonan WT, Andringa A, Doetschman T, Manning PA, Liu LH, Miller ML, Shull GE.** Impaired renal NaCl absorption in mice lacking the ROMK potassium channel, a model for type II Bartter's syndrome. *J Biol Chem* 277: 37871–37880, 2002.
22. **Lu M, Wang T, Yan Q, Yang X, Dong K, Knepper MA, Wang W, Giebisch G, Shull GE, Hebert SC.** Absence of small conductance K^+ channel (SK) activity in apical membranes of thick ascending limb and cortical collecting duct in ROMK (Bartter's) knockout mice. *J Biol Chem* 277: 37881–37887, 2002.
23. **MacVinish LJ, Guo Y, Dixon AK, Murrell-Lagnado RD, Cuthbert AW.** Xe^{991} reveals differences in K^+ channels regulating chloride secretion in murine airway and colonic epithelium. *Mol Pharmacol* 60: 753–760, 2001.
24. **Neyroud N, Tesson F, Denjoy I, Leibovici M, Donger C, Barhanin J, Faure S, Gary F, Coumel P, Petit C, Schwartz K, Guicheney P.** A novel mutation in the potassium channel gene KVLQT1 causes the Jervell and Lange-Nielsen cardioauditory syndrome. *Nat Genet* 15: 186–189, 1997.
25. **Plotkin MD, Kaplan MR, Verlander JW, Lee WS, Brown D, Poch E, Gullans SR, Hebert SC.** Localization of the thiazide sensitive Na-Cl cotransporter, rTSC1 in the rat kidney. *Kidney Int* 50: 174–183, 1996.
26. **Priori SG, Barhanin J, Hauer RN, Haverkamp W, Jongsma HJ, Kleber AG, McKenna WJ, Roden DM, Rudy Y, Schwartz K, Schwartz PJ, Towbin JA, Wilde A.** Genetic and molecular basis of cardiac arrhythmias: impact on clinical management. Study Group on Molecular Basis of Arrhythmias of the Working Group on Arrhythmias of the European Society of Cardiology. *Eur Heart J* 20: 174–195, 1999.
27. **Sambrook J, Fritsch EF, Maniatis T.***Molecular Cloning: A Laboratory Manual*. Cold Spring Harbor, NY: Cold Spring Harbor Laboratory Press, 1989.
28. **Sangan P, Rajendran VM, Mann AS, Kashgarian M, Binder HJ.** Regulation of colonic H-K-ATPase in large intestine and kidney by dietary Na depletion and dietary K depletion. *Am J Physiol Cell Physiol* 272: C685–C696, 1997.
29. **Schulze-Bahr E, Wang Q, Wedekind H, Haverkamp W, Chen Q, Sun Y, Rubie C, Hordt M, Towbin JA, Borggrefe M, Assmann G, Qu X, Somberg JC, Breithardt G, Oberti C, Funke H.** KCNE1 mutations cause Jervell and Lange-Nielsen syndrome. *Nat Genet* 17: 267–268, 1997.
30. **Splawski I, Tristani-Firouzi M, Lehmann MH, Sanguinetti MC, Keating MT.** Mutations in the hminK gene cause long QT syndrome and suppress I_{Ks} function. *Nat Genet* 17: 338–340, 1997.
31. **Teng-umnuay P, Verlander JW, Yuan W, Tisher CC, Madsen KM.** Identification of distinct subpopulations of intercalated cells in the mouse collecting duct. *J Am Soc Nephrol* 7: 260–274, 1996.
32. **Tsevi I, Vicente R, Grande M, Lopez-Iglesias C, Figueras A, Capella G, Condom E, Felipe A.** KCNQ1/KCNE1 channels during germ-cell differentiation in the rat: expression associated with testis pathologies. *J Cell Physiol* 202: 400–410, 2005.
33. **Vallon V, Grahammer F, Richter K, Bleich M, Lang F, Barhanin J, Volkl H, Warth R.** Role of KCNE1-dependent K^+ fluxes in mouse proximal tubule. *J Am Soc Nephrol* 12: 2003–2011, 2001.
34. **Vallon V, Grahammer F, Volkl H, Sandu CD, Richter K, Rexhepaj R, Gerlach U, Rong Q, Pfeifer K, Lang F.** KCNQ1-dependent transport in renal and gastrointestinal epithelia. *Proc Natl Acad Sci USA* 102: 17864–17869, 2005.
35. **Verlander JW, Hassell KA, Royaux IE, Glapion DM, Wang ME, Everett LA, Green ED, Wall SM.** Deoxycorticosterone upregulates PDS (Slc26a4) in mouse kidney: role of pendrin in mineralocorticoid-induced hypertension. *Hypertension* 42: 356–362, 2003.
36. **Verlander JW, Madsen KM, Low PS, Allen DP, Tisher CC.** Immunocytochemical localization of band 3 protein in the rat collecting duct. *Am J Physiol Renal Fluid Electrolyte Physiol* 255: F115–F125, 1988.
37. **Verlander JW, Miller RT, Frank AE, Royaux IE, Kim YH, Weiner ID.** Localization of the ammonium transporter proteins RhBG and RhCG in mouse kidney. *Am J Physiol Renal Physiol* 284: F323–F337, 2003.
38. **Verlander JW, Moudy RM, Campbell WG, Cain BD, Wingo CS.** Immunohistochemical localization of H-K-ATPase α_{2c}-subunit in rabbit kidney. *Am J Physiol Renal Physiol* 281: F357–F365, 2001.
39. **Verlander JW, Tran TM, Zhang L, Kaplan MR, Hebert SC.** Estradiol enhances thiazide-sensitive NaCl cotransporter density in the apical plasma membrane of the distal convoluted tubule in ovariectomized rats. *J Clin Invest* 101: 1661–1669, 1998.
40. **Wall SM, Hassell KA, Royaux IE, Green ED, Chang JY, Shipley GL, Verlander JW.** Localization of pendrin in mouse kidney. *Am J Physiol Renal Physiol* 284: F229–F241, 2003.
41. **Wang Q, Curran ME, Splawski I, Burn TC, Millholland JM, VanRaay TJ, Shen J, Timothy KW, Vincent GM, de JT, Schwartz PJ, Toubin JA, Moss AJ, Atkinson DL, Landes GM, Connors TD, Keating MT.** Positional cloning of a novel potassium channel gene: KVLQT1 mutations cause cardiac arrhythmias. *Nat Genet* 12: 17–23, 1996.
42. **Wang Z, Li H, Moss AJ, Robinson J, Zareba W, Knilans T, Bowles NE, Towbin JA.** Compound heterozygous mutations in KvLQT1 cause Jervell and Lange-Nielsen syndrome. *Mol Genet Metab* 75: 308–316, 2002.
43. **Wingo CS, Madsen KM, Smolka A, Tisher CC.** H-K-ATPase immunoreactivity in cortical and outer medullary collecting duct. *Kidney Int* 38: 985–990, 1990.
44. **Wingo CS, Smolka AJ.** Function and structure of H-K-ATPase in the kidney. *Am J Physiol Renal Fluid Electrolyte Physiol* 269: F1–F16, 1995.
45. **Xia SL, Teng X, Wingo CS.** Nucleotides induced Ca-dependent ion transport in mIMCD-3 cells (Abstract). *Mol Biol Cell* 14: 82A, 2003.
46. **Zhou X, Wingo CS.** Stimulation of total CO_2 flux by 10% CO_2 in rabbit CCD: role of an apical Sch-2. *Am J Physiol Renal Fluid Electrolyte Physiol* 267: F114–F120, 1994.
47. **Zhou X, Xia SL, Wingo CS.** Chloride transport by the rabbit cortical collecting duct: dependence on H,K-ATPase. *J Am Soc Nephrol* 9: 2194–2202, 1998.